A four-dimensional quantum mechanical state-to-state study of the $H_2+C_2H\rightarrow H+C_2H_2$ reaction

Henrik Szichman, Miquel Gilibert, Miguel González, Xavier Giménez, and Antonio Aguilar[a)]
Department de Química Física i Centre de Recerca en Química Teòrica, Universitat de Barcelona, C/Martí i Franquès 1, 08028 Barcelona, Spain

(Received 27 November 2000; accepted 5 March 2001)

A quantum mechanical approach to treat diatom–triatom exchange processes of the type $AB+CDE\rightarrow A+BCDE$ is presented. The initial nine degree-of-freedom problem is simplified to a reaction having active only five of such degrees of freedom, which emulates a rotating–stretching *AB* molecule colliding colinearly with a linear *CDE* molecule. This model is then applied to study the $H_2+C_2H\rightarrow H+C_2H_2$ reaction. In the present work, the H_2 rotations are treated using the infinite-order-sudden-approximation (IOSA) method, whereas the coupled states (CS or j_z) approximation is employed to uncouple the total angular momentum **J** from internal rotations. Thus, a four-dimensional mathematical analysis is performed, which allows the computation of state-to-state reactive probabilities and cross sections. The bending vibrational levels of the acetylene C_2H_2 molecule are calculated on the basis of a one single degenerate bending expansion, i.e., just one H (the attacked one) is considered to bend, the remainder being frozen. Present results show that the product acetylene is formed in highly excited vibrational states, particularly if either the reacting asymmetric CH or symmetric C_2 stretches are involved. Finally, rate constant results are compared with two other theoretical treatments and with experiments. © *2001 American Institute of Physics.* [DOI: 10.1063/1.1367387]

I. INTRODUCTION

An infinite-order-sudden-approximation (IOSA) quantum mechanical (QM) methodology has been recently used to study the title reaction.[1] This work was based on the calculation of all nonreactive probabilities, the sum of which is then subtracted from unity to obtain the total reactive probability.[2–5] Thus, all computations were carried out on the reagents arrangement channel (AC) only. Despite the computational convenience of such an analysis, it obviously lacks the capability of discerning between the different product energy states. In the present article, our attention is drawn conversely to the following reactive state-to-state process:

$$H_2(j_1,n_1=0)+C_2H(n_2\bar{j}n_2'=0|j_2,m_2=0)$$
$$\rightarrow H+C_2H_2(\nu_1\bar{\nu}\nu_2 b_1 b_2|K\Omega_K),$$
$$\Delta H_0=-31.0\ \text{kcal mol}^{-1}. \quad (1)$$

Here, j_1,n_1 are the rotational and vibrational quantum numbers of the H_2 diatomic molecule and $n_2,\bar{j}$ and n_2' are, respectively, the symmetric, bending, and asymmetric quantum numbers of the C_2H radical. In our calculations, we will assume these numbers to be in their ground-state values. As for the products, the acetylene C_2H_2 molecule is characterized by seven quantum numbers, i.e., ν_1, $\bar{\nu}$, and ν_2 are the symmetric, symmetric CC stretch, and asymmetric vibrational quantum numbers, whereas b_1 and b_2 correspond to two bending modes. Additionally, K and Ω_K (and j_2,m_2) represent, respectively, the (overall) rotational number and its projection of the tetra(tri)-atom molecule on a body-fixed penta-atomic frame. The reader may note that all the bending modes involved in the above reaction (1) are doubly degenerate.

Obtaining the bending quantum wave functions for the acetylene C_2H_2 molecule, is a demanding theoretical as well as computational task. Besides the problem of double degeneracy, the computational resources needed are extensive, even prohibitive for the actual reaction. In order to cope with this problem,[6] and specifically with the title system,[7] Bowman and co-workers have proposed the application of the so-called ''bending energy shift approximation.'' Such an approach implies certain assumptions about the harmonicity of the bending oscillations involved in the reaction, as well as on the accuracy of the *J*-shift approximation. Assessing these ideas is one of the aspects also treated in this work, being more related to structural features rather than to the explicit reactive process.

In the present work we devised a halfway approach between Bowman's approximation and the full bending solution, so that reasonably accurate results for the rate constants might be obtained (as in the case of Refs. 1 and 7): we envision, in this model, a bend-frozen ethynyl C_2H radical colliding in a linear trajectory with a rotating H_2 stretch, one H of the H_2 bond reacting then with the C_2H molecule. As for the product description, we developed the bend-

a)Author to whom correspondence should be addressed. Electronic mail: antonio@qf.ub.es

vibrational energy level scheme of C_2H_2, by means of a quantum one single degenerate bend expansion (QOSDBE)[8,9] (we avoided the consideration of the double degeneracy aspect, since we estimate it to be less relevant given the coplanarity assumptions used in this work).

The calculations are performed on the Wang and Bowman HC_2H_2 potential energy surface (PES) published elsewhere,[7] as in our previous study.[1]

The work is organized as follows. In Sec. II we review the theoretical QM methodology employed in this work. In Sec. III we give the QM numerical details of the calculations. The results and discussion are provided in Sec. IV, and Sec. V is for the summary.

II. FIVE-ATOM QM-IOSA THEORY

The basic theory that stands behind the present approach is not different from that already published for triatom and tetra-atom systems,[8–11] which, in practice, is valid for any polyatomic system. Our main aim with the numerical calculations is to obtain the transition (reactive) *S*-matrix elements,

$$S(t_\nu \leftarrow t_{0\lambda}) = \frac{1}{i\hbar}\langle \psi_{t_\nu} | V_\nu | \Psi_{t_{0\lambda}} \rangle \rangle, \tag{2}$$

where ψ_{t_ν} is the unperturbed (asymptotic) quantum-state wave function in the product AC and V_ν is the relevant perturbation potential, meanwhile $\Psi_{t_{0\lambda}}$ represents the total wave function. Here, $(\alpha=\nu,\lambda)$ stand for the (products, reagents) ACs and t_α represents the quantum number sets describing a given state in an α AC. The remaining reactive quantities of interest, such as state-to-state probabilities, cross sections, rotational distributions, and finally rate constants, may then be obtained via Eq. (2), by means of standard formulas.[8]

Obtaining ψ_{t_α} requires solving the following Schrödinger equations (SEs):

$$(E-H_\alpha)\psi_{t_\alpha}=0, \tag{3}$$

where H_α are the unperturbed (elastic) Hamiltonians in both ACs. On the other hand, the total wave function $\Psi_{t_{0\lambda}}$, which is the solution of the full Hamiltonian *H*, is split, in a perturbative spirit, into the addition of two parts:

$$\Psi_{t_{0\lambda}} = \psi_{t_{0\lambda}} + \chi_{t_{0\lambda}}. \tag{4}$$

It can be easily shown, by elementary algebra, that the perturbed part $\chi_{t_{0\lambda}}$ can be obtained by solving the following inhomogenuous SE in the close-interaction region:

$$(E-H)\chi_{t_{0\lambda}} = V_\lambda \psi_{t_{0\lambda}}. \tag{5}$$

Here V_α are the interaction (perturbation) potentials in each AC, conventionally defined by

$$V_\alpha = H - H_\alpha. \tag{6}$$

In actual calculations, *H* is replaced by H_I, which is similar to *H*, but contains also the required negative imaginary potentials (NIPs), so as to supply the necessary absorbing boundary conditions. Throughout the present study, NIPs of the Neuhauser–Baer linear ramp type[12] were used.

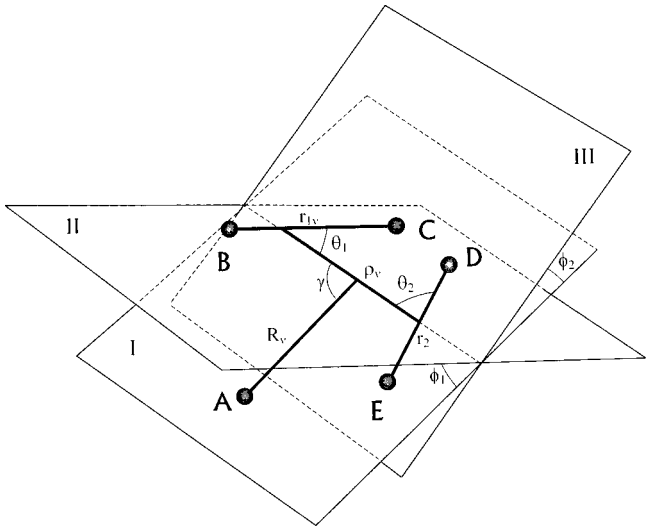

FIG. 1. The nine Jacobi coordinates for the atom–tetra-atom (products) AC studied in the present work.

The present treatment differs in several aspects from those cited above for triatom and tetra-atom systems.[8–11] First, it is the use of a ϕ (out-of-plane angle)-averaged PES in the reagents AC, even though this feature becomes irrelevant for the title reaction, because of its linear arrangement. The second difference is the use of a discretional grid, instead of a random selection rule, to treat the IOSA angle γ_1 (see Fig. 3 below).

A. The products AC: Atom–tetra-atom Hamiltonian

The coordinate description of an atom+tetra-atom molecule can be performed in two ways, according to the manner in which the tetra-atom is represented. The latter can be configured in a diatom–diatom arrangement or in an atom–triatom (atom–diatom) one.[8,9,13] One could assume that the final result should not depend on the type of representation adopted. This may be rigorous in full-dimensional studies, but no longer holds in approximate treatments. For instance, different dimensionality reductions lead to sampling different portions of the PES. Furthermore, the PES itself may have been designed within some preconceived configuration. Thus, it becomes rather convenient to choose a favorable representation for the atom+tetra-atom system in study. In the present case, an atom-diatom–diatom configuration proves to be the most convenient way to represent the product penta-atomic system. This configuration is shown in Fig. 1.

The tetra-atom BCDE (in our case C_2H_2) is described then as the coupling of two (CH) bonds, BC and DE, for which the vibrational coordinates are indicated, respectively, by $r_{1\nu}$ and r_2 (see Fig. 1). In the same figure, the coordinate ρ_ν, connecting the centers of mass of these two last bonds, is the corresponding ''translational'' distance of the diatom–diatom configuration. Finally, the fourth and last radial distance is assigned to the translational coordinate R_ν, which connects the center of mass of the tetra-atom, placed somewhere on the distance ρ_ν, with the fifth center of the penta-atomic molecule. Five Jacobi angles then complete the description of the system, where three of them are the

azimuthal angles: θ_1 and θ_2 (the angles sustained, respectively, between $r_{1\nu}$ and r_2, and ρ_ν); and γ (the angle between R_ν and ρ_ν). In order to introduce the two additional polar angles β_1 and β_2 we consider the plane defined by the distances R_ν and ρ_ν (indicated by an I in Fig. 1) as the reference plane of the atom–tetra-atom system. The other two planes characterizing this system are those defined by the distance ρ_ν and each one of the vibrational coordinates $r_{1\nu}$ and r_2. Both planes are indicated by II and III, respectively, in the same figure, Fig. 1. Finally, ϕ_1 and ϕ_2 are the polar angles between the (I,II) and (I,III) planes, respectively.

The calculation of $\psi_{t_{0\nu}}$ (and its full expression in the strong interaction region) may be performed considering the following Hamiltonian in body-fixed coordinates, for a given total angular momentum **J**:

$$H_\nu = -\frac{\hbar^2}{2\mu_{1\nu}r_{1\nu}}\cdot\frac{\partial^2}{\partial r_{1\nu}^2}r_{1\nu} - \frac{\hbar^2}{2\mu_2 r_2}\cdot\frac{\partial^2}{\partial r_2^2}r_2 - \frac{\hbar^2}{2\mu_\nu\rho_\nu}\cdot\frac{\partial^2}{\partial\rho_\nu^2}\rho_\nu - \frac{\hbar^2}{2M_\nu R_\nu}\cdot\frac{\partial^2}{\partial R_\nu^2}R_\nu + \frac{\hbar^2}{2\mu_{1\nu}r_{1\nu}^2}\cdot\mathbf{j}_{1\nu}^2 + \frac{\hbar^2}{2\mu_2 r_2^2}\cdot\mathbf{j}_2^2 + \frac{\hbar^2}{2\mu_\nu\rho_\nu^2}\cdot(\mathbf{K}-\mathbf{j}_{12})^2 + \frac{\hbar^2}{2M_\nu R_\nu^2}(\mathbf{J}-\mathbf{K})^2 + U(r_{1\nu}r_2\rho_\nu R_\nu\theta_1\phi_1\theta_2\phi_2\gamma). \tag{7}$$

In Eq. (7), $\mu_{1\nu}$ and μ_2 are, respectively, the reduced masses of the BC and DE stretches, and μ_ν and M_ν those of the tetra-atom and the atom–tetra-atom systems. $\mathbf{j}_{1\nu}$ and $\mathbf{j}_2$ represent the bending angular momentum operators of the tetra-atom molecule, which partially couple to give $\mathbf{j}_{12}$, meanwhile **K** is the total angular momentum operator of the tetra-atom system. Finally, the full PES U is expressed as functionally depending on the nine dynamic variables shown in Fig. 1. As for the orbital angular momentum operators $(\mathbf{K}-\mathbf{j}_{12})$ and $(\mathbf{J}-\mathbf{K})$, the j_z approximation is applied,[14] so they become

$$(\mathbf{K}-\mathbf{j}_{12})^2 = K(K+1) + \mathbf{J}_{12}^2 - 2\Omega_K^2 \tag{8}$$

and

$$(\mathbf{j}-\mathbf{K})^2 = J(J+1) + K(K+1) - 2\Omega_\nu^2, \tag{9}$$

where Ω_K is the projection of both **K** and $\mathbf{j}_{12}$ along ρ_ν, whereas Ω_ν stands for the equivalent quantity for **J** and **K** along R_ν. $\mathbf{j}_{12}$ results from the coupling between $\mathbf{j}_{1\nu}$ and $\mathbf{j}_2$. In the present model, its square modulus is approximated as

$$\mathbf{j}_{12}^2 = \mathbf{j}_{1\nu}^2 + \mathbf{j}_2^2 + 2\Omega_{1b}\cdot\Omega_{2b}, \tag{10}$$

where Ω_{1b} and Ω_{2b} are, respectively, the projections of $\mathbf{j}_{1\nu}$ and $\mathbf{j}_2$ over ρ_ν. It can be seen that the following relation holds:

$$\Omega_K = \Omega_{1b} + \Omega_{2b}. \tag{11}$$

Equations (10) and (11) may be combined and replaced in Eq. (8) to give

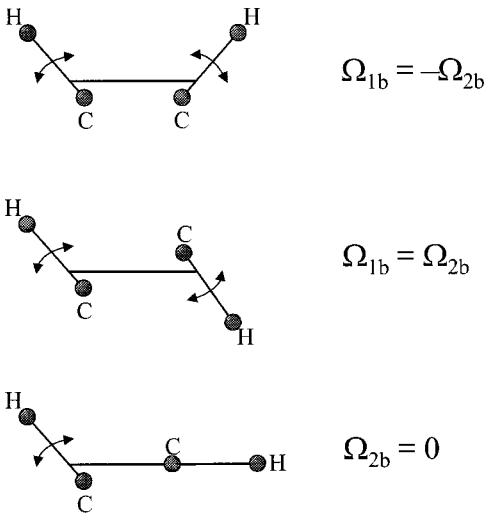

FIG. 2. Schemes for the acetylene C_2H_2 z-projected configurations, as discussed in this study.

$$(\mathbf{K}-\mathbf{j}_{12})^2 = K(K+1) + \mathbf{j}_{1\nu}^2 + \mathbf{j}_2^2 - 2[\Omega_K^2 - (\Omega_K - \Omega_{2b})\cdot\Omega_{2b}]. \tag{12}$$

Equation (12) depends on two precession quantum numbers, which are necessary in order to preserve all the degrees of freedom of the penta-atomic molecule. Nevertheless, in symmetrical systems like the present, one may expect that the projections of $\mathbf{j}_{1\nu}^2$ and $\mathbf{j}_2^2$ on an equidistant z axis should be equal in modulus, i.e., $\Omega_{1b} = \pm\Omega_{2b}$. Note that when one of the CH stretch bending is frozen, as it is considered here, $\Omega_{2b} = 0$. The implications of these configurations on the acetylene molecule are schematized in Fig. 2.

As for U (denoted as U_ν in the asymptotic region ν), it is assumed to adopt the following form:[9]

$$U_\nu(r_{1\nu}r_2\rho_\nu R_\nu\theta_1\theta_2|\phi_1\phi_2\gamma) = v_\nu(r_{1\nu}r_2\rho_\nu\theta_1\theta_2|\phi_1\phi_2) + w_\nu(R_\nu|\phi_1\phi_2\gamma), \tag{13}$$

where v_ν is the potential of the isolated tetra-atom, meanwhile w_ν is the νth distortion potential, which is assumed to behave like a van der Waals intermolecular potential. Both potentials are calculated according to the following expressions:

$$v_\nu(r_{1\nu}r_2\rho_\nu\theta_1\theta_2|\phi_1\phi_2) = \lim_{R_\nu\to\infty} U(r_{1\nu}r_2\rho_\nu R_\nu\theta_1\theta_2\phi_1\phi_2\gamma) \tag{14}$$

and

$$w_\nu(R_\nu|\phi_1\phi_2\gamma) = U(r_{1\nu e}r_{2e}\rho_{\nu e}R_\nu\theta_{1e}\theta_{2_e}|\phi_1\phi_2\gamma), \tag{15}$$

where U is again the full penta-atomic potential, expressed in terms of the ν coordinates, and $r_{1\nu e}$, r_{2e}, $\rho_{\nu e}$, θ_{1e}, and θ_{2e} are the equilibrium coordinates for the tetra-atomic molecule. In the present case, they are obtained from the minimization of the HC_2H_2 potential energy surface at the asymptotic region $(R_\nu = \infty)$.

In what follows we assume that **K**, $\mathbf{j}_2 \equiv \mathbf{0}$ and, consequently, $\Omega_K = \Omega_\nu = \Omega_{2b} = 0$. Furthermore, since a ''colinear'' collision is considered, $\gamma = \theta_2 = \phi_1 = \phi_2 = 0$, so that

they will be omitted in the formulas henceforth. We observe, since the U_ν potential is separable, that the solution of Eq. (3) can be written as

$$\psi_{o\nu}(r_{1\nu}r_2\rho_\nu R_\nu\theta_1|\nu_1\overline{\nu}\nu_2\overline{b}J) = \frac{1}{r_{1\nu}r_2\rho_\nu R_\nu}\phi_{o\nu}(r_{1\nu}r_2\rho_\nu\theta_1|\nu_1\overline{\nu}\nu_2\overline{b}) \times\zeta_{o\nu}(R_\nu|\nu_1\overline{\nu}\nu_2\overline{b}J), \tag{16}$$

where $\psi_{o\nu}(r_{1\nu}r_2\rho_\nu R_\nu\theta_1|\nu_1\overline{\nu}\nu_2\overline{b})$ are the eigenfunctions [with eigenvalues $\epsilon(\nu_1\overline{\nu}\nu_2\overline{b})$] of the equation[15]

$$\left[-\frac{\hbar^2}{2\mu_{1\nu}}\frac{\partial^2}{\partial r_{1\nu}^2}-\frac{\hbar^2}{2\mu_2}\frac{\partial^2}{\partial r_2^2}-\frac{\hbar^2}{2\mu_\nu}\frac{\partial^2}{\partial\rho_\nu^2} + \frac{\mathbf{j}_{1\nu}^2}{2}\left(\frac{1}{\mu_{1\nu}r_{1\nu}^2}+\frac{1}{\mu_\nu\rho_\nu^2}\right)+v(r_{1\nu}r_2\rho_{1\nu}\theta_1) - \epsilon(\nu_1\overline{\nu}\nu_2\overline{b})\right]\phi_{o\nu}(r_{1\nu}r_2\rho_\nu\theta_1\theta_2|\nu_1\overline{\nu}\nu_2\overline{b})=0, \tag{17}$$

meanwhile $\zeta_{o\nu}(R_\nu|\nu_1\overline{\nu}\nu_2\overline{b}J)$ are the solutions of the equation

$$\left(-\frac{\hbar^2}{2\mu_\nu}\cdot\frac{\partial^2}{\partial R_\nu^2}+\frac{\hbar^2}{2\mu_\nu}\frac{J(J+1)}{R_\nu^2}+w_\nu(R_\nu) - \frac{\hbar^2}{2\mu_\nu}k^2(\nu_1\overline{\nu}\nu_2\overline{b})\right)\zeta_{o\nu}(R_\nu|\nu_1\overline{\nu}\nu_2\overline{b}J)=0. \tag{18}$$

Here $k(\nu_1\overline{\nu}\nu_2\overline{b})$ is the standard wave number, defined by

$$k(\nu_1\overline{\nu}\nu_2\overline{b})=\left(\frac{2\mu_\nu}{\hbar^2}[E-\epsilon(\nu_1\overline{\nu}\nu_2\overline{b})]\right)^{1/2}. \tag{19}$$

Calculated eigenvalues for this C_2H_2 (the product) AC in the ground bend state (GBS) and in the one single degenerate bending expansion are presented in Table I. These energies are listed relative to the zero-point energy of C_2H_2 located, according to the present calculations, 0.6253 eV below the minimum of the H_2+C_2H potential. The implications of these values will be discussed later in the following sections.

The reader may note that for a general case when $\mathbf{K}\neq 0$, allowing the C_2H_2 molecule to rotate as a rigid bar, the expression in Eq. (16) should be multiplied by $d^K_{\Omega_K\Omega_\nu}(\gamma)$, the representation of the rotation matrix with respect to the $\mathbf{R}_\nu$ axis.[16]

B. The reagents AC: Diatom–triatom Hamiltonian

A diatom+triatom, as any other penta-atom molecule, is fully characterized by ten interatomic distances related univocally to nine degrees of freedom. Four of the latter are spent in translational–vibrational modes, three in bend–rotational ones, and two in orbital precession motion.[1] Following previous works on tetra-atom systems,[8] a Jacobi coordinate system has been chosen to describe the reagent AC of the present five-atom system (see Fig. 3). Thus, the diatom–triatom (reagent) channel is described by four radial distances and five Jacobi angles. More explicitly, the coordinate assignment begins first with the triatom CDE (in our case, the radical C_2H). It is described within an atom–diatom configuration.[15,17] It then follows a diatom stretch AB(H_2), for which the vibrational coordinate is indicated in Fig. 3 by $r_{1\lambda}$. The atom–diatom configuration includes the same vibrational coordinate r_2 for the DE bond as in Fig. 1 (in most cases remaining as a ''*spectator*'') and the corresponding ''*translational*'' coordinate of the triatom ρ_λ connecting the extreme atom C with the center of mass of the bond DE. Finally, the fourth radial distance is assigned to the translational coordinate R_λ, which connects the center of mass of the diatom AB and the triatom's center of mass, placed somewhere on the distance ρ_λ. Five Jacobi angles then complete the description of the system, where three of them are the azimuthal angles: θ (the angle sustained between r_2 and ρ_λ); and γ_1 and γ_2 (the angles between R_λ and the respective coordinates $r_{1\lambda}$ and ρ_λ). In order to introduce the two additional polar angles β_1 and β_2, the plane defined by the distances R_λ and ρ_λ (indicated by I in Fig. 3) is the origin for the Euler angle representation and will be used as the reference plane of the diatom–triatom system. Two other planes characterize this system: one is the that defined by the distances $(R_\lambda, r_{1\lambda})$ and the other is the triatomic plane. Both planes are indicated by II and III, respectively, in Fig. 3. Finally, β_1 is the polar angle between planes (I,II) and β_2 between (I,III).

The full calculation of $\psi_{t_{0\lambda}}$ (and $\chi_{t_{0\lambda}}$) requires considering the following Hamiltonian, in body-fixed coordinates, for a given total angular momentum $\mathbf{J}$:[1]

$$H=-\frac{\hbar^2}{2\mu_{1\lambda}r_{1\lambda}}\cdot\frac{\partial^2}{\partial r_{1\lambda}^2}r_{1\lambda}-\frac{\hbar^2}{2\mu_2 r_2}\cdot\frac{\partial^2}{\partial r_2^2}r_2 - \frac{\hbar^2}{2\mu_\lambda\rho_\lambda}\cdot\frac{\partial^2}{\partial\rho_\lambda^2}\rho_\lambda-\frac{\hbar^2}{2M_\lambda R_\lambda}\cdot\frac{\partial^2}{\partial R_\lambda^2}R_\lambda+\frac{\hbar^2}{2\mu_{1\lambda}}\cdot\frac{\mathbf{j}_1^2}{r_{1\lambda}^2} + \frac{\hbar^2}{2}\cdot\mathbf{j}^2\left(\frac{1}{\mu_2 r_2^2}+\frac{1}{\mu_\lambda\rho_\lambda^2}\right)+\frac{\hbar^2}{2\mu_\lambda}\frac{\mathbf{j}_2^2}{\rho_\lambda^2}+\frac{\mathbf{l}_\lambda^2}{2M_\lambda R_\lambda^2} + U(r_{1\lambda}r_2\rho_\lambda R_\lambda\theta|\gamma_1\gamma_2\beta_1\beta_2). \tag{20}$$

In Eq. (20), $\mu_{1\lambda}$ is the reduced mass of the AB bond, and μ_λ and M_λ correspond to those of the triatom and the diatom–triatom systems, respectively. $\mathbf{j}_1$ and $\mathbf{j}_2$ are the rotational angular momentum operators of the diatom and triatom, respectively, whereas $\mathbf{j}$ stands for the bending angular momentum operator of the triatomic molecule. $\mathbf{l}_\lambda$ is the total orbital angular momentum operator of the diatom–triatom system. Finally, the full PES U depends on the nine dynamic variables shown in Fig. 3. As for $\mathbf{l}_\lambda$, once the j_z approximation is applied,[14]

$$\mathbf{l}_\lambda^2=\hbar^2[J(J+1)+J_\lambda(J_\lambda+1)-2\Omega^2], \tag{21}$$

where Ω is the projection of the total angular momentum on R_λ and J_λ (resulting from the coupling between j_1 and j_2), is an integer assumed to lie in the range $|j_1-j_2|\leqslant J_\lambda\leqslant|j_1+j_2|$.

The Hamiltonian defined in Eq. (20) is then slightly altered, obtaining H_λ and H_I, so as to calculate, respectively, the asymptotic (unperturbed) elastic wave function $\psi_{t_{0\lambda}}$ and

TABLE I. A comparison of C_2H_2 calculated vibrational–bend energies in the ground bend state (GBS) and in a one single degenerated bend expansion (OSDBE). Energies are expressed in cm^{-1} and assigned using a conventional normal mode $(\nu_s\nu_{CC}\nu_a;b)$. Note that in fact, the present bending numbers refer to the even degenerated states, so they should be multiplied by two for their proper labeling.

		Present				Present	
$(\nu_s\nu_{CC}\nu_a;b)$	Ref. 7	GBS	OSDBE	$(\nu_s\nu_{CC}\nu_a;b)$	Ref. 7	GBS	OSDBE
(000;1)			1322.63	(111;0)	8482.14	8724.10	8240.55
(010;0)	2063.31	2130.15	2107.10	(100;4)			8250.51
(000;2)			2641.33	(021;1)			8325.13
(001;0)	3206.51	3140.90	3074.00	(010;5)			8501.19
(100;0)	3378.79	3334.19	3335.38	(210;0)	8713.62	8875.00	8601.04
(010;1)			3355.61	(120.1;)			8614.29
(000;3)			3938.56	(002;2)			8657.76
(020;0)	4115.49	4154.67	4163.69	(030;2)			8754.19
(001;1)			4221.00	(101;2)			8862.13
(100;1)			4540.41	(011;3)			8864.79
(010;2)			4661.71	(200;2)			8892.35
(011;0)	5251.11	4850.61	4820.08	(031;0)	9329.02		
(000;4)			5184.57	(003;0)	9397.57	9477.03	9083.51
(110;0)	5410.81	5479.91	5359.73	(110;3)			9119.30
(020;1)			5463.14	(031;0)		9697.02	9161.05
(001;2)			5535.39	(020;4)			9270.87
(100;2)			5646.12	(102;0)	9448.39	9793.92	9340.25
(010;3)			5976.86	(130;0)	9550.82	9832.30	9346.64
(030;0)	6166.54			(012;1)			9485.30
(002;0)	6343.18	6274.85	6054.05	(001;5)			
(030;0)		6431.13	6158.83	(201;0)	9631.47	9926.05	9609.06
(101;0)	6427.86	6565.04	6331.05	(040;1)			9612.04
(011;1)			6376.03	(111;1)			9648.83
(000;5)			6507.29	(100;5)			9724.12
(200;0)	6633.53	6686.15	6522.46	(300;0)	9879.89	10 245.19	9761.70
(110;1)			6689.95	(021;2)			9767.79
(020;2)			6698.48	(010;6)			9847.31
(001;3)			6723.12	(210;1)			9868.05
(100;3)			6914.02	(120;2)			9876.97
(021;0)	7288.45	7086.77	7127.09	(002;3)			9946.51
(010;4)			7174.22	(030;3)			10005.23
(120;0)	7477.18	7515.02	7226.93	(101;3)			10078.36
(002;1)			7267.60	(050;0)	10 277.52		
(030;1)			7357.42	(022;0)	10 400.92	10 301.83	10 116.34
(101;1)			7498.53	(011;4)			10 183.22
(011;2)			7250.76	(200;3)			10 301.78
(000;6)			7636.28	(050;0)		10 490.59	10 310.48
(200;1)			7783.69	(121;0)	10 534.81	10 834.50	10 357.64
(110;2)			7806.48	(003;1)			10 372.82
(020;3)			7862.80	(110;4)			10 375.49
(012;0)		7899.71	7872.38	(031;1)			10 422.92
(001;4)			8020.56	(020;5)			10 518.07
(040;0)	8221.63	8283.23	8146.42	(220;0)	10 793.71	10 852.69	10 571.59
(012;0)	8372.45						

$\chi_{t_{0\lambda}}$ [Eq. (3) and Eq. (5)]. Note that H_λ differs from the full Hamiltonian H by the fact that the full PES in the latter should be replaced by the expression of the out-of-plane-averaged (unperturbed) potential energy surface in the former. It is given by the elastic addition of the separate vibrational, bend–vibrational, and translational energy components:

$$\overline{U}_\lambda(r_{1\lambda}r_2\rho_\lambda R_\lambda\theta|\gamma_1\gamma_2)=v_1(r_{1\lambda})+v_2(r_2\rho_\lambda\theta)+\overline{w}(R_\lambda|\gamma_1\gamma_2), \tag{22}$$

where $v_1(r_{1\lambda})$ and $v_2(r_2\rho_\lambda\theta)$ are the potential energy surface for the H_2 and C_2H molecules, which follow from

$$v_1(r_{1\lambda})=\lim_{R_\lambda\to\infty} U(r_{1\lambda}r_{2e}\rho_{e\lambda}R_\lambda\theta_e\gamma_1\gamma_2\beta_1\beta_2) \tag{23}$$

and

$$v_2(r_2\rho_\lambda\theta)=\lim_{R_\lambda\to\infty} U(r_{1e\lambda}r_2\rho_\lambda R_\lambda\theta\gamma_1\gamma_2\beta_1\beta_2). \tag{24}$$

Finally, the distortion potential $\overline{w}(R_\lambda|\gamma_1\gamma_2)$ may be defined as

$$\overline{w}(R_\lambda|\gamma_1\gamma_2)=\overline{U}(r_{1e\lambda}r_{2e}\rho_{e\lambda}R_\lambda\theta_e\gamma_1\gamma_2). \tag{25}$$

Note that $r_{1e\lambda}$, r_{2e}, $\rho_{e\lambda}$, and θ_e are obtained from the equilibrium properties of the H_2 and C_2H molecules, which are an integral part of the HC_2H_2 potential energy surface.

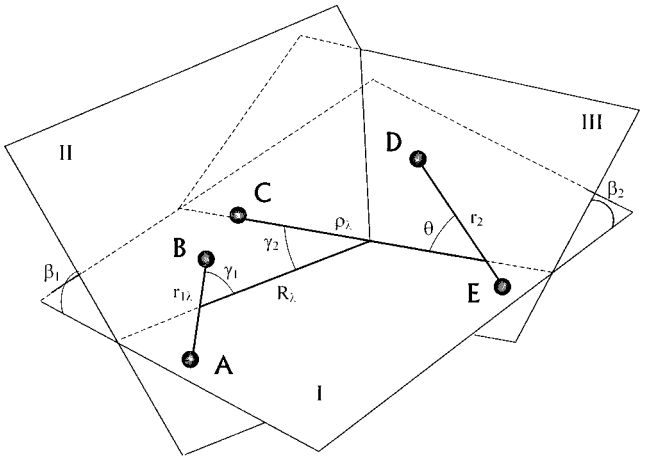

FIG. 3. The nine Jacobi coordinates for the diatom–triatom (reagents) AC employed for the calculations in the present work.

In the present ''colinear'' application case, the linearity of C_2H makes unnecessary averaging over β_2 (see Fig. 3) and, since $\gamma_2=0$, $\overline{w}$ simply reduces to

$$\overline{w}(R_\lambda|\gamma_1\gamma_2)=U(r_{1e\lambda}r_{2e}\rho_{e\lambda}R_\lambda\theta_e=0\,\gamma_1\gamma_2=0\beta_1\beta_2). \tag{26}$$

Furthermore, since the $\overline{U_\lambda}$ potential is separable in terms of all variables, the solution of Eq. (3) for the reagents channel, in the present case, can be written as

$$\psi_{o\lambda}(r_{1\lambda}r_2\rho_\lambda\theta_e R_\lambda\gamma_1|j_1t_1t_2J)$$
$$=\frac{1}{r_{1\lambda}r_2\rho_\lambda R_\lambda}\phi_{o\lambda}^{(1)}(r_{1\lambda}|t_1)\phi_{o\lambda}^{(2)}(r_2\rho_\lambda\theta_e|t_2)$$
$$\times\zeta_{o\lambda}(R_\lambda|t_1t_2J)y(\gamma_10|t_1), \tag{27}$$

where $\phi_{o\lambda}^{(i)}$, $(i=1,2)$ are the λ vibrational eigenfunctions of the H_2 diatom and C_2H triatom, respectively, t_1 and t_2 standing for their initial quantum number conditions. $\zeta_{o\lambda}$ are the corresponding translational components. They all fulfill equations similar to Eqs. (17)–(18), for the products AC. Finally, $y(\gamma_10|j_1)$ is a spherical harmonic denoting the initial rotational state of H_2, characterized by the quantum number j_1. In the present application of our IOSA model, we assume this initial rotating state to be kept along the whole reactive process. The eigenvalues characterizing the input channel for reaction (1), as calculated in the present work using the HC_2H_2 PES of Ref. 7, are shown in Table II. They are given relative to the minimum of the H_2+C_2H potential.

TABLE II. Vibrational energies/eV of $H_2(\nu)+C_2H(\nu_{CC}\nu_{CH})$ calculated in the ground bend state.

ν	$(\nu_{CC}\nu_{CH})$	$H_2(\nu)+C_2H(\nu_{CC}\nu_{CH})$
0	00	0.601
	10	0.840
	01	1.014
	20	1.076
1	00	1.116
0	11	1.252
	30	1.308
1	10	1.355
0	02	1.430
	21	1.486

C. Derivation of the perturbed function χ_{λ_0}

The function χ_{λ_0} is derived by solving Eq. (5) in the reagents AC. For that purpose, the range(s) of the reagents vibrational coordinate(s) are enlarged such as to include the relevant reactive regions and the necessary decoupling NIPs. In the present system, the radical C_2H is assumed to behave almost as a spectator during the process $H_2+C_2H\rightarrow H+C_2H_2$. Hence, it is incorrect to place NIPs at the edges of the coordinate ranges for r_2 or ρ_λ. We must include rather one NIP at the translational distance R_λ, in order to ensure the boundary conditions in this direction, and another one in the reactive bond $r_{1\lambda}$, namely

$$V_I(r_{1\lambda}r_2\rho_\lambda R_\lambda\gamma_1)\equiv -i[v_{Ir_{1\lambda}}(r_{1\lambda})+v_{IR_\lambda}(R_\lambda)]. \tag{28}$$

The Hamiltonian H_I in Eq. (5) depends on five Jacobi coordinates, according to the assumptions of the present model. Four of them are the distances $r_{1\lambda}$, r_2, ρ_λ, and R_λ, meanwhile the fifth coordinate is the angle γ_1. In our work, the radial distances are treated as continuous variables, but the angle γ_1 is considered as an IOSA parameter. A five-dimensional (5-D) analysis was not attempted here, not only because of computational restraints, but also because the H's in the HC_2H_2 PES,[7] are not fully interchangeable between them, and this fact does not allow this type of study. It follows then that each 4-D calculation is to be carried out for fixed values of the angle γ_1 and then averaged over the range $0\leqslant\gamma_1\leqslant\pi/2$.

Following our description of the derivation of $\chi_{0\lambda}$, we note that since the whole treatment is to be carried out in the λ AC for a fixed Jacobi angle γ_1, we shall drop henceforth from the following notation the index λ and γ_1 will be denoted as γ.

Adding the two NIPs to the real potential U converts the scattering problem into a bound-type problem. Consequently χ_{λ_0} can be expanded in terms of square integrable L^2 functions.[18–20] These are chosen as localized functions for the translational components and adiabatic basis sets for the three vibrational coordinates.[21,22] Thus χ_{λ_0} may be written as[21,22]

$$\chi_{0\lambda}^J(r_1r_2\rho R|\nu_1\overline{\nu}\nu_2\overline{b}|\gamma j_1t_1t_2)$$
$$=\frac{1}{r_1r_2\rho R}\sum_{nt}a_{nt}^J(\nu_1\overline{\nu}\nu_2\overline{b}|\gamma j_1t_1t_2)$$
$$\times g_n(R)f_{nt}(r_1r_2\rho|\gamma j_1). \tag{29}$$

Here $g_n(R)$ is the localized Gaussian function,[21,22]

$$g_n(R)=\left(\frac{\alpha}{\sigma\sqrt{\pi}}\right)^{1/2}\exp\left[-\frac{\alpha^2}{2}\left(\frac{R-R_n}{\sigma}\right)^2\right], \tag{30}$$

where R_n $(n=0,...,N)$ are $N+1$ equidistant sectors along the translational axis R, α is a fitted dimensional parameter, and σ is the grid size,

$$\sigma = R_n - R_{n-1}. \tag{31}$$

As for $f_{nt}(r_1 r_2 \rho | \gamma j_1)$, it is an eigenfunction of the equation

$$\left(-\frac{\hbar^2}{2\mu_1}\cdot\frac{\partial^2}{\partial r_1^2} - \frac{\hbar^2}{2\mu_2}\cdot\frac{\partial^2}{\partial r_2^2} - \frac{\hbar^2}{2\mu}\cdot\frac{\partial^2}{\partial \rho^2} + \frac{\hbar^2}{2}\cdot\frac{j_1(j_1+1)^2}{\mu_1 r_1^2} + U(r_1 r_2 \rho R = R_n | \gamma) - \epsilon_t(j_1 | R_\nu) \right) f_{nt}(r_1 r_2 \rho | \gamma j_1) = 0, \tag{32}$$

where $\epsilon_t(j_1|R_n)$ is the corresponding tth eigenvalue related to the eigenstates of Eq (32).

The a_{nt}^J coefficients are obtained from the solution of Eq. (5) followed by the substitutions implied by Eqs. (27)–(29). Once these a_{nt}^J coefficients are known and replaced in Eq. (29) to compute $\chi_{0\lambda}$, the scattering elements $S^J(t_\nu \leftarrow t_{0\lambda}, j_1)$ can be calculated by means of Eq. (2), brought under the form

$$S^J(t_\nu \leftarrow t_{0\lambda}, j_1) = \frac{1}{i\hbar}\left(\langle \psi_{o\nu}^J | V_\nu | \psi_{o\lambda, j_1}^J \rangle + \sum_{nt} a_{nt}^J \langle \psi_{o\nu} | V_\nu | g_n f_{nt} y(\gamma 0 | j_1) \rangle \right). \tag{33}$$

Formally f_{nt} should include an explicit dependence on the angular momentum basis function $y(\gamma 0|j_1)$. Since this spherical harmonic function gets a constant value due to the IOSA constraint, its inclusion in Eq. (29) is irrelevant because it will cancel at the matrix inversion implied in Eq. (5), irrespective of its value. Nevertheless, its inclusion is important in the calculation of the scattering matrix elements and thus it is shown explicitly in Eq. (33).

Finally, once the J-specific-averaged reaction probabilities are obtained, the QM state-to-state reactive cross sections are calculated by using

$$\sigma(\nu_1 \overline{\nu} \nu_2 \overline{b} \leftarrow j_1 t_1 t_2) = \frac{\pi}{k^2(E_{\rm tr})} \sum_J (2J+1) \times |S^J(\nu_1 \overline{\nu} \nu_2 \overline{b} \leftarrow j_1 t_1 t_2)|^2, \tag{34}$$

where $k(E_{\rm tr})$ is the standard wave number for the whole diatom+triatom system, which is defined by $k^2(E_{\rm tr}) = (2M/\hbar^2)E_{\rm tr}$.

III. NUMERICAL DETAILS

As specified, reactive cross sections given in Eq. (34) were obtained for the exchange process of reaction (1). State-to-state cross sections have been calculated for one initial state, namely, the ground state of H_2+C_2H and for ~42 final vibrational states, where $(\nu_1, \overline{\nu}, \nu_2)$ range between (0, 0, 0) and (4, 6, 4). These results are the sum of $\overline{b}$ bend–folded calculations with $\overline{b}$ ranging between 0 to 6. This set of calculations were finally repeated for a series of values of $E_{\rm tr}$, ranging from 0.025 to 0.400 eV, with the purpose of estimating relevant temperature-dependent rate constants for reaction (1).

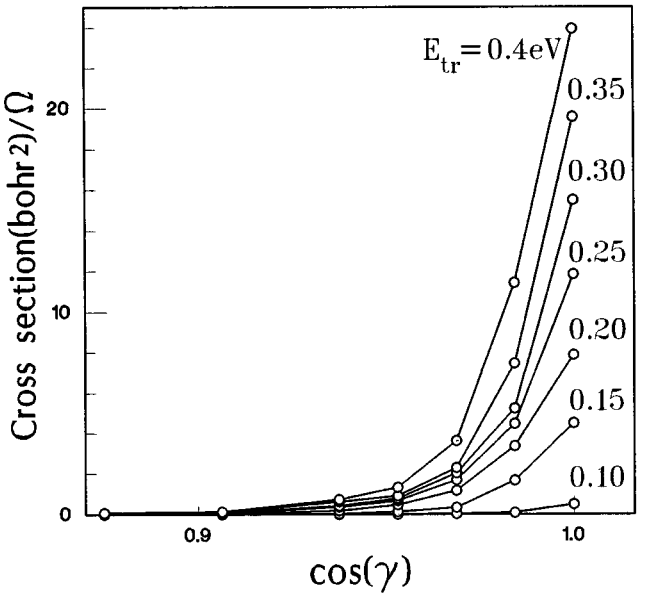

FIG. 4. The distribution of calculated integral cross sections for reaction (1) as a function of the incidence $\cos(\gamma)$. Curves shown were calculated for different values of $E_{\rm tr}$ ranging from 0.10 to 0.40 eV in steps of 0.05 eV, as indicated in the figure.

The calculations, in general, were done within the j_z approximation, but in order to derive χ (the perturbed part of the total wave function in the reagents' AC), the IOSA, which *a priori* is believed to be valid for high energies, was employed. The χ function is, nevertheless, essentially nonzero along a short translational interval only and, consequently, it is expected to be valid for low energies too. The IOSA is applied, as stated, by considering the angle γ as a parameter rather than a continuous coordinate. Consequently, each S-matrix element (or transition probability) is obtained following an averaging process carried out over a discretional grid of cos (γ) in the range $0 \leqslant \gamma \leqslant \pi/2$ (For a γ distribution of the computed integral cross section for different values of $E_{\rm tr}$, see Fig. 4).

In order to get well-converged IOSA results, the translational range was taken from 1.85 to 4.8 Å. The translational NIP was 1 Å long and 0.5 eV height. This translational axis was divided into 50 equidistant sectors, in which the corresponding equations are solved [see Eqs. (29)–(32)]. One Gaussian as a translational basis function, plus a set of adiabatic three-mode vibrational basis functions [see Eq. (32)] were attached to each sector. As a general rule, the adiabatic sets were determined by a two-step procedure: first, an adiabatic basis set for each one of the (three) internal coordinates (a sinus set to describe vibrational motions and spherical harmonics for the bend oscillations) is used. The remaining (two) internal coordinates are assumed to adopt their equilibrium values. In the second, using part of these basis functions, a global basis set is formed. The number of adiabatic basis functions adopted to describe the breaking bond H_2 were 12 out of 30 and 10 out of 30 for the C_2 stretch. The vibration of the remaining bond CH was described less rigorously, as it is assumed not to participate in the reaction process, due to its ''spectator'' character. Thus, 1 out of 20 basis functions were used in our calculations to describe the

TABLE III. Convergence tests at $E_{tr}=0.4$ eV of C_2H_2 calculated total vibrational reactive cross sections $\times 1000$ (in bohr^2), for a different number of adiabatic functions describing the motion of the nonreactive CH strecth in the short range interaction region. The reactants C_2H+H_2 are considered being initially in the rovibrational ground-state.

	N (CH)		
$(\nu_s \nu_{CC} \nu_a)$	1	2	3
(0,0,0)	6.822	6.538	6.675
(0,1,0)	7.957	7.887	7.984
(0,0,1)	15.261	21.159	20.445
(1,0,0)	10.609	10.973	10.866
(0,2,0)	18.438	22.246	21.845
(0,1,1)	10.429	9.652	10.487
(1,1,0)	3.394	3.801	3.878
(0,0,2)	18.435	19.704	19.601
(0,3,0)	12.987	14.153	13.693
(1,0,1)	5.984	6.582	6.707
(2,0,0)	5.277	5.211	5.058
(0,2,1)	10.586	11.121	11.102
(1,2,0)	8.014	8.681	8.590
(0,1,2)	5.243	7.048	7.392
(0,4,0)	4.030	5.197	5.134
(1,1,1)	4.861	4.655	4.792
(2,1,0)	9.026	10.436	11.188
(0,0,3)	2.626	2.547	2.449
(0,3,1)	10.507	11.195	12.095
(1,0,2)	4.048	4.458	4.012
(1,3,0)	3.760	2.951	2.866
(2,0,1)	5.262	5.013	5.073
(3,0,0)	7.037	6.422	6.448
(0,2,2)	1.022	1.420	1.362
(0,5,0)	6.329	8.013	7.447
(1,2,1)	3.503	4.974	5.149
(2,2,0)	4.861	5.176	5.163
(0,1,3)	1.051	1.143	1.014
(0,4,1)	1.164	1.387	1.265
(1,1,2)	4.057	4.432	4.437
(1,4,0)	2.738	2.395	2.279
(2,1,1)	0.881	1.025	0.998
(3,1,0)	2.445	3.325	3.073
(0,0,4)	0.320	0.389	0.384
(0,3,2)	8.046	7.928	7.889
(1,0,3)	0.671	0.515	0.473
(0,6,0)	0.627	0.388	0.406
(1,3,1)	0.274	0.135	0.138
(2,0,2)	0.753	0.654	0.654
(2,3,0)	0.700	0.759	0.769
(3,0,1)	0.002	0.003	0.002
(4,0,0)	0.000	0.000	0.000
TOTAL	230.175	251.592	251.349

motion of the end diatom. Nevertheless, full computations for the cross sections at a single translational energy ($E_{tr}=0.4$ eV) were carried out using a different number of basis functions see Table III. The number of these global functions varied from one sector to another, being determined by a given cutoff energy value (2.2 eV in the present study; also see the discussion in Ref. 20). This procedure led, in the most unfavorable case treated here, to about 2500 (complex) equations that had to be solved for each value of γ. The solutions of these equations were obtained employing the lower–upper (LU) decomposition method.[23]

The vibrational range corresponding to the breaking bond (H_2) had the turning points placed at 0.4 and 2.5 Å along the r_1 distance, being the vibrational NIP 1 Å long again, whereas the linear ramp height was 0.12 eV. The range of ρ and r_2 (the nonreactive bonds) were taken, respectively, as (0.60–1.8 Å) and (0.60–1.4 Å). The equations of the asymptotic (unperturbed) region for the products AC [Eq. (20)] have been solved using the (2.10–4.50 Å) and (0.80–1.60 Å) ranges for R_ν and ρ_{1v}, respectively. Additionally, a set of adiabatic bend–triply vibrational basis functions was built in order to obtain converged eigenvalues for the relevant energy states of C_2H_2. For this purpose, a set of 6 and 18 eigenfunctions were used to describe the CH and C_2 stretches, and 7 for the bending oscillations.

The equations for each energy and each gamma are also solved for relevant values of the total angular momentum J. The results for each value of J are then summed up, according to Eq. (34), to yield cross sections at given values of the total energy and γ. The maximum value of J taken in account depends on γ and the translational energy considered. The highest value corresponds to $J=50$ with $\gamma=0$ and $E_{tr}=0.4$ eV.

IV. RESULTS AND DISCUSSION

The vibrational energies of C_2H_2 in the ground bend state (GBS) and in a one single degenerate bend expansion (OSDBE) have already been presented in Table I. They are compared with previous calculations of Wang and Bowman (WB),[7] performed using the same HC_2H_2PES. GBS, and WB approaches to the energy levels differ only in numerical aspects, which cause the disagreement of a few percent shown in Table I. Our main concern is, however, the comparison between GBS and OSDBE, since they are based on fairly different physical assumptions for the bending motion. A reasonable agreement between both calculations is obtained. The reader may note that a set of conventional normal mode quantum numbers, v_s, v_{CC}, v_a, referring to the symmetric, CC, and antisymmetric stretches, respectively, have been used to label the vibrational states, in conformance with Ref. 7, whereas the single bend mode b is that considered from the v_a side.

The present calculations evidence the notorious anharmonicity of the vibrational energy eigenvalues. The GBS energy spacing shrinks with increasing the stretching quantum numbers but, conversely, the bend mode spacing slightly increases with the bending quantum number. This latter feature is a clear manifestation of the hindered rotational character of the bending motion. A relevant coupling is obtained between the bending modes and the GBS ones, measured as the energy difference between the results obtained with and without inclusion of the bending motion. The coupling is largest for levels where v_a is excited (being the side from which the bend mode is expanded). The addition of the second bending may increase, presumably, this coupling. These facts should be taken into account when comparing the present results with those from the bending energy shift approximation.

Table II shows the calculations done for the vibrational energies of H_2+C_2H (in the ground bend state). The agreement with WB is much better, so that only the present results are shown. We note in this respect that our energy values do

not include the normal bend mode of C_2H. But since this exclusion is done for both the reactant and product sides, it is assumed that the error will approximately cancel out, unaffecting the final results.

In Fig. 4 the calculated γ-dependent integral cross sections for different values of E_{tr} are presented, ranging from 0.10 to 0.40 eV in steps of 0.05 eV. The colinear dominancy of the title reaction may be appreciated, with a conical angle of acceptance to the reaction of no more than 25°. This dominancy increases with energy, but only in relative terms, since the quotient between colinear and noncolinear cross sections increases with energy. However, in absolute terms, a widening of the cone of acceptance is observed with increasing energy, as the cross section goes up with energy for noncolinear angles. This feature is fairly common for colinearly dominated reactions and is simply explained in terms of the energy available to the reaction.

The computation of cross sections shown in Fig. 4, as elsewhere in this paper unless explicitly stated, was done employing one adiabatic basis function to describe the vibration of the nonreactive CH bond, as it is assumed to act as a ''spectator'' in the reaction process. We checked these assumptions by carrying out full state-to-state cross section computations at one single translational energy, using a higher number of basis functions. The results obtained for $E_{tr}=0.4$ eV are shown in Table III, where the number of adiabatic basis functions $[N(\mathrm{CH})]$ used varied from 1 to 3. Note that the listed results apply to the vibrational states of C_2H_2, after being obtained through a sum over their bend sub-states. On inspection of this table it may be concluded that using one adiabatic function is already a good approximation, since the total cross section only varies by 10%. The relative distribution of the state-to-state cross sections is also kept over the different $N(\mathrm{CH})$, despite the fact that some transitions, like those corresponding to the states (0, 0, 1) and (0, 2, 0), seem to be boosted rather than inhibited, as more vibrational functions of the nonreactive CH are taken into account.

Figure 5 shows calculated integral cross sections for reaction (1) as a function of translational energy E_{tr} and the *b*-bend quantum number. It is appreciated that for low E_{tr} values, the curves are seen to cross over, due to the high coupling existing between them. Conversely, the tendency at larger energies is that the curves become ordered in a decreasing way by increasing *b*. This is expected from the analysis of Fig. 4 and the fulfillment of IOSA collision conditions. At a given (sufficiently high) translational energy, one obtains a lower reactivity for higher bending quantum numbers, if one correlates higher *b* values with larger oscillation amplitudes for the bending motion and thus the sampling of higher bending angles. This leads to lower reactivity as the bending angle is larger, since the time spent in large, less reactive angles is higher as the bending quantum number increases. This ''geometric'' factor then dominates the collision outcome, as the different bending states do not effectively couple during the course of the collision, at high energies (IOSA-type collision).

Table IV shows *b*-summed state-to-state cross section calculations, between 0.050 and 0.400 eV, in steps of 0.050

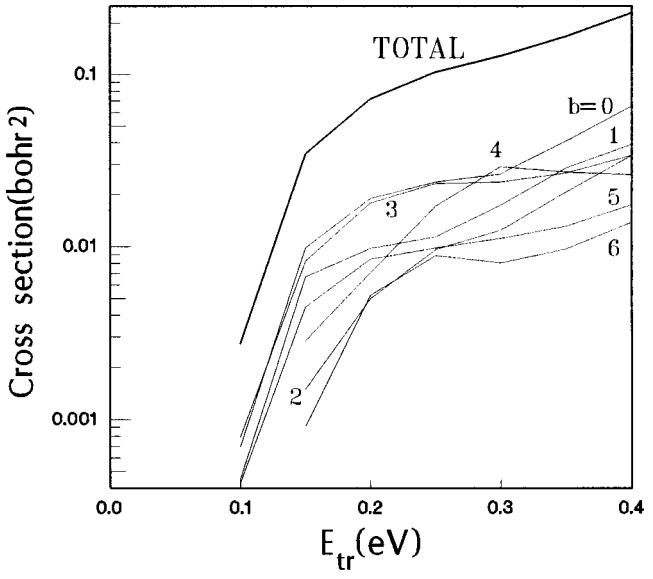

FIG. 5. The distribution of calculated integral cross sections for reaction (1) as a function of the translational energy E_{tr} according to their *b*-bend composition.

eV. In order to facilitate their interpretation, Figs. 6 and 7 show the distribution of state-to-state cross sections along the vertical columns of Table IV, at translational energies of $E_{tr}=0.15$ and 0.40 eV, respectively. Figure 8, whereas, displays the contents of the same table along the horizontal rows, showing the variation of the state-to-state cross sections with energy.

The reliability of the present results may be first assessed by comparing them with those of Wang and Bowman, even though the latter were obtained for the reverse reaction and, more important, using a different methodological approach. The main result of Wang and Bowman is a remarkable reaction selectivity, for the excitation of the asymmetric C_2H_2 mode leads to an important cross section enhancement, but only when the CC stretch is simultaneously excited. Other conclusions from this study are the noticeable degree of nonadiabaticity for the CC stretch, as well as the small cross sections for simulataneous excitation of the symmetric and asymmetric vibrations.

The main product state in the WB results is, in most cases, the ground state for H_2+C_2H, i.e., our initial state in the present calculations. A comparison between both studies is then consistent, the only change being that reaction selectivity, in WB, converts to reaction especificity, for the present results. This comparison leads to the fact that some features are in agreement, but for others a marked disagreement is obtained. Thus, both the nonadiabaticity of the CC stretch and the small cross sections for symmetric–asymmetric excitations are features common to both approaches. Conversely, the simultaneous asymmetric-CC excitation leads to reactivity inhibition in the present study, in opposition to the WB enhancement. The present calculations show a dominant role of the CC stretch, as for product distributions: four out of the five highest state-to-state cross sections are participated by this vibration at low energy (0.15 eV), whereas five out of eight apply at the highest energy

TABLE IV. A comparison of C_2H_2 calculated total vibrational reactive cross sections $\times 1000$ (in $bohr^2$) for different translational energies of the reactants C_2H+H_2 that are considered being initially in the rovibrational ground state.

	E /eV							
$(\nu_s \nu_{CC} \nu_\alpha)$	0.050	0.100	0.150	0.200	0.250	0.300	0.350	0.400
(0,0,0)	0.000	0.022	0.210	0.385	0.333	0.594	3.399	6.822
(0,1,0)	0.000	0.050	0.470	0.632	0.571	1.142	4.851	7.957
(0,0,1)	0.001	0.392	4.422	10.377	13.332	11.892	12.042	15.261
(1,0,0)	0.001	0.142	1.770	3.924	3.770	4.214	6.773	10.609
(0,2,0)	0.001	0.127	1.414	3.653	4.905	6.078	10.931	18.438
(0,1,1)	0.001	0.103	1.490	3.200	3.965	4.507	6.538	10.429
(1,1,0)	0.002	0.488	2.615	3.034	3.661	4.185	3.938	3.394
(0,0,2)	0.001	0.094	0.898	3.069	10.978	19.784	18.801	18.435
(0,3,0)	0.000	0.161	3.485	9.742	14.137	14.684	13.305	12.987
(1,0,1)	0.000	0.032	0.661	1.203	1.636	3.103	4.696	5.984
(2,0,0)	0.000	0.052	1.000	2.557	3.212	2.596	3.349	5.277
(0,2,1)	0.001	0.128	1.054	2.111	4.089	5.395	7.794	10.586
(1,2,0)	0.001	0.084	0.916	1.478	2.683	4.011	5.935	8.014
(0,1,2)	0.000	0.018	0.668	2.336	3.737	3.742	4.291	5.243
(0,4,0)	0.000	0.082	0.611	0.879	0.978	1.010	2.171	4.030
(1,1,1)	0.000	0.072	1.271	2.462	2.579	2.277	2.879	4.861
(2,1,0)	0.001	0.306	3.790	4.269	4.035	4.831	6.106	9.026
(0,0,3)	0.000	0.026	0.372	0.823	1.303	1.927	2.453	2.626
(0,3,1)	0.001	0.108	1.496	2.612	2.262	3.065	6.681	10.507
(1,0,2,)	0.000	0.067	0.840	1.384	1.779	1.829	2.358	4.048
(1,3,0)	0.000	0.000	0.070	0.395	0.707	0.851	1.897	3.760
(2,0,1)	0.000	0.040	1.203	2.352	2.701	2.736	4.342	5.262
(3,0,0)	0.000	0.087	0.956	1.791	4.370	5.290	5.348	7.037
(0,2,2)	0.000	0.001	0.034	0.155	0.373	1.070	1.249	1.022
(0,5,0)		0.001	0.081	0.381	0.859	3.410	5.540	6.329
(1,2,1)		0.049	2.466	5.416	5.642	4.032	3.545	3.503
(2,2,0)		0.000	0.180	1.456	2.858	2.920	3.358	4.861
(0,1,3)			0.000	0.098	0.543	0.916	0.824	1.051
(0,4,1)				0.039	0.417	0.816	0.712	1.164
(1,1,2)				0.032	1.075	3.400	3.937	4.057
(1,4,0)				0.001	0.200	0.931	2.007	2.738
(2,1,1)					0.121	0.711	1.015	0.881
(3,1,0)					0.001	0.406	1.508	2.445
(0,0,4)						0.008	0.154	0.320
(0,3,2)						0.002	2.204	8.046
(1,0,3)							0.075	0.671
(0,6,0)							0.093	0.627
(1,3,1)							0.028	0.274
(2,0,2)							0.014	0.753
(2,3,0)								0.700
(3,0,1)								0.002
(4,0,0)								0.000
TOTAL	0.012	2.732	34.460	72.306	103.846	128.377	167.018	230.175

explored in the present study (0.4 eV). Consequently, the enhancing role played by the CC stretch appears to be a common feature between the results of WB and the present results. Thus, it is only the *combined* asymmetric-CC effect which is found to be in contradiction between both methodologies.

Furthermore, it is interesting to note that the WB selectivity enhancement rate, which is *ca.* 50 at 0.4 eV between the $(003) \rightarrow (00)+(0)$ and the $(013) \rightarrow (00)+(0)$ transitions, is much higher than any specificity enhancement rate found in the present calculations, the highest being *ca.* 6 at the same translational energy, for transitions involving reasonably close (in energy) final vibrational levels.

A further comparison between Figs. 6–8 opens the possibility of figuring out the mechanism prevailing in the reactive process of reaction (1). It is as follows: the rotating H_2 stretch hits head-on the ethynyl C_2H radical, causing the creation of the C_2H_2 molecule by abstraction of one H from the H_2 diatom. The latter is likely to be in a highly vibrationally excited state, in order to facilitate the breaking of the bond and initiate the reaction. This is concluded from the fact that up to 12 and 10 basis functions (for H_2 and CC respectively) were necessary, in the strong interaction region, to converge the calculations (cf. Sec. III). Thus, one reactive H adheres the ethynyl radical to give the resulting C_2H_2 with the attacked CH stretch being in a high vibrational level. Later on, by relaxation of this CH, an energy transfer takes place to the CC and the second remote CH bonds. This process is clearly observed in Fig. 6, showing the results for $E_{tr}=0.15$ eV,

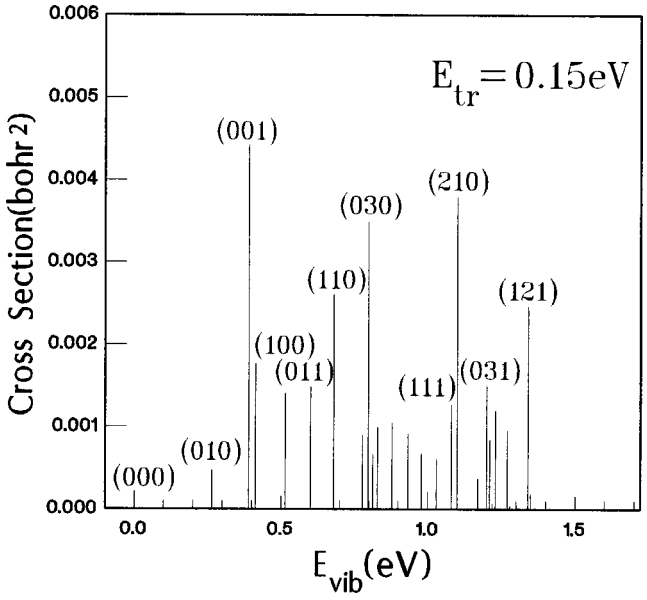

FIG. 6. The distribution of calculated vibrational state-to-state cross sections for reaction (1) for constant translational energy $E_{tr}=0.15$ eV (see Table IV).

meanwhile for $E_{tr}=0.40$ eV (see Fig. 7) the relaxation of the frontal CH is more difficult, remaining in its highly excited state and almost not reaching its far symmetrical counterpart.

From Fig. 8, we have learned that reaction (1) happens with a certain final state especificity, up to translational energies of about 0.4 eV. Within this range, the final C_2H_2 states of pure excited CH or CC stretches are preferred. Beyond $E_{tr}=0.40$ eV, a tendency toward equating the population is guessed, for the acetylene vibrational levels, so that, presumably, the reaction could be studied by statistical theories.

Finally, QM rate constants have been calculated from total cross sections using the following expression:[24]

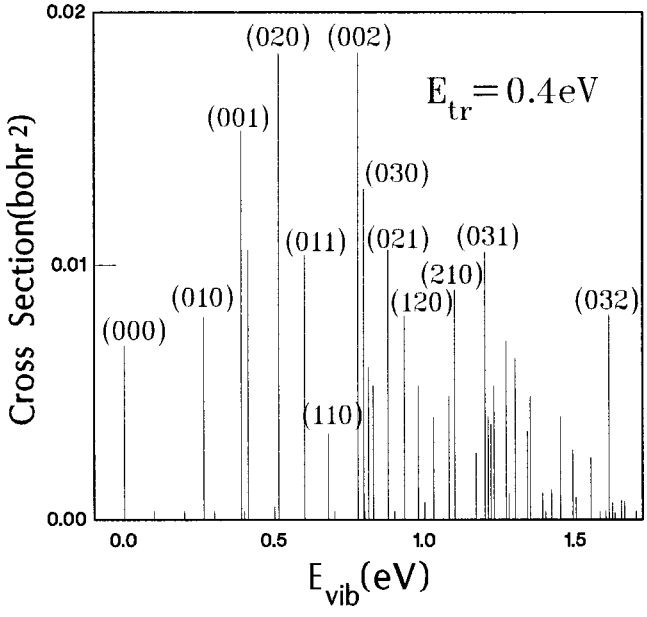

FIG. 7. The same as Fig. 6 for $E_{tr}=0.40$ eV.

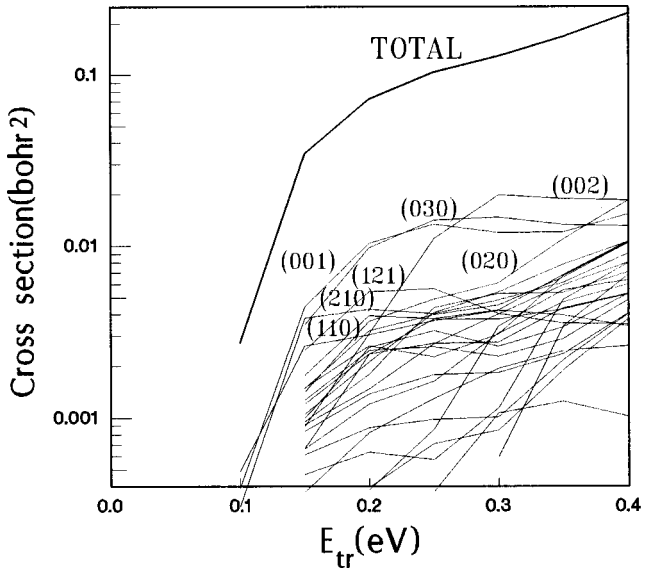

FIG. 8. The distribution of calculated vibrational state-to-state cross sections for reaction (1) as a function of the translational energy E_{tr} (see Table IV).

$$k=\left(\frac{1}{k_BT}\right)^{3/2}\left(\frac{8}{\pi M}\right)^{1/2}\int_0^\infty E_T\sigma(E_T)e^{-E_T/k_BT}\,dE_T, \quad (35)$$

where k_B is the known Boltzmann gas constant and M is the already defined M_λ, the reduced mass of the diatom+triatom system in Eq. (20). The so computed rate constant values are presented in Fig. 9. They are compared,

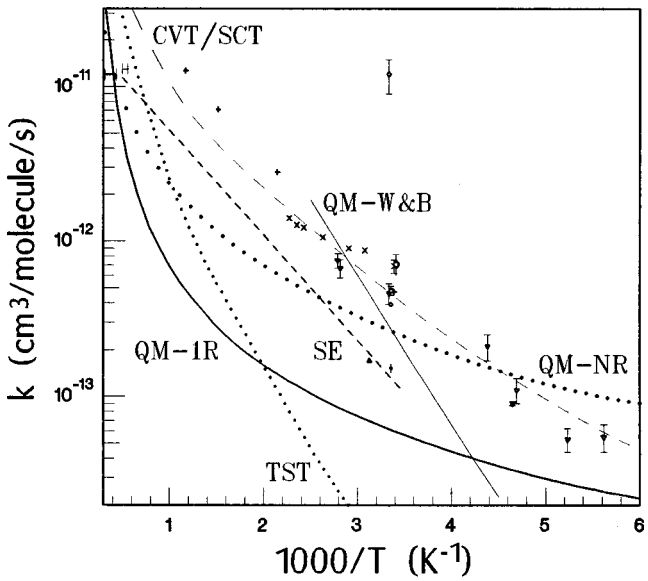

FIG. 9. An Arrhenius plot of the rate constant k vs 1000 K/T for the title reaction. (a) A full line (—) indicates the present results (QM-1R); (b) a heavy dotted line (···) represents nonreactive (QM-NR) (Ref. 1) predictions; (c) light line (—) QM-W&B (Ref. 7) ones; (d) a light dotted line (···) represents classical transition state theory (TST) calculations (Ref. 25); (e) a Heavy dashed line (– – –) is a semiempirical (SE) recommended curve (from Ref. 27); (f) a light dashed line (– – –) represents CVT/SCT prediction (from Ref. 26); (g) a experimental points indicated as a triangle (△) (Ref. 28); dot (●) (Ref. 29); diamond (◇) (Ref. 30); open dot (○) (Ref. 31); light dash (1–) (Ref. 32); heavy dash (–) (Ref. 33); square (□) (Ref. 34); hexagon (⬡) (Ref. 35); down triangle (▽) (Ref. 37); cross (+) (Ref. 36); and (×) (Ref. 38).

in the same figure, with similar results obtained by different theoretical methods,[1,7,25,26] as well as with experimental data.[27–38]

We estimate the present result to fall short from that of Ref. 1 (indicated as QM-NR in Fig. 9) by a factor of ~4. A factor 2, because only one bend is considered and another factor of 2 because only one extreme CH bond is mainly excited. The main feature of this figure is, besides this out-of-scale factor, that the present results for the Arrhenius plot (indicated as QM-1R in Fig. 9) show practically the same dynamical behavior than that of Ref. 1. This tendency is in good agreement with the latest experimental data[35–38] and further corroborated by recent theoretical results obtained using the canonical variational transition state method (with small curvature tunneling corrections) (CVT/STC).[26] These results were obtained directly by means of a variational method that does not yield an analytical expression for the PES, as required in the present dynamical treatment. The reader should then be aware that both results may refer to different potential energy surfaces. On the other hand, the differences between our QM results and the calculations reported in Ref. 7 (QM-W&B in the same figure) should be explained in terms of the different methodologies applied.

V. SUMMARY AND CONCLUSIONS

A quantum mechanical approach to treat processes like the title reaction was developed. First, this approach was presented with its nine degrees of freedom, but further on simplified to one having active only five of them. The resulting model emulates a rotating stretch H_2 colliding colinearly with a linearly arranged ethynyl C_2H molecule. The rotations of the H_2 were treated using an IOSA-type approach, meanwhile the CS or j_z approximation was employed to uncouple the total angular momentum **J** from internal rotational operators. Thus, a four mathematical dimensional analysis was done in order to compute state-to-state reactive probabilities and cross sections. For that purpose, the quantum vibrational–bend energy levels of the acetylene C_2H_2 molecule were calculated on the basis of a one single degenerated bend expansion. Present results showed that the product C_2H_2 molecules are formed in high vibrational states, particularly if the asymmetric (reacting) CH or symmetric C_2 stretches are involved. In this way, a strong inversion of population for the different vibrational levels is thus produced. This finding is in good agreement with calculations done in Ref. 7, where in order to promote reactivity for the opposite reaction, high excitation of the vibrational states was necessary. The effect of simultaneously exciting the CC and asymmetric stretches has been found, conversely, to inhibit rather than to enhance the reaction.

Finally, rate constant results were compared with those from other treatments and from experiments. The present results were found a factor of 4 lower than previous nonreactive calculations,[1] according to our expectations given the restrictions adopted in this work, affecting the degrees of freedom of the penta-atomic system. It is remarkable to note, nevertheless, that the dynamics properties of the present calculated Arrhenius curve, shown in Fig. 9, coincide practically with those predicted by the QM-NR calculations, increasing in this way our discrepancies with the QM-W&B results. These discrepancies should be clearly attributed to the different methodological approaches, since they are based on two different dimensionality reduction schemes.

In this respect, it is worth citing recent QM studies on polyatomic systems[39–41] to conclude that, for the time being, the direct confrontation among different QM models, applied to high polyatomic systems, is the best way to assess their underlying theoretical foundations. Additionally, results presented here show that state-to-state analyses are necessary to provide a detailed insight on the reaction mechanism, which is somewhat hidden if canonical flux-correlation methods are used,[26,41] since only the global rate constant is available in these cases.

ACKNOWLEDGMENTS

H.S. was on leave from the Department of Physics and Applied Mathematics, Soreq NRC, Israel, and thanks the ''Profesores visitantes de IBERDROLA'' program and CEPBA for a visiting professor fellowship. The support of the Spanish Ministry of Education and Science (MEC), Projects No. PB97-0919 and No. PB98-1209-C02-01, as well as the ''Center de Supercomputació i Comunicacions de Catalunya, C^4-CESCA'' for computer time made available is also gratefully acknowledged.

[1] H. Szichman, M. Gilibert, M. González, X. Giménez, and A. Aguilar, J. Chem. Phys. **113**, 176 (2000).
[2] H. Szichman, A. J. Varandas, and M. Baer, J. Chem. Phys. **102**, 3474 (1995).
[3] M. Baer, H. Szichman, E. Rosenman, S. Hochman-Kowal, and A. Perski, in *Springer Series in Chemical Physics, Vol. 61, Gas Phase Chemical Reaction Systems*, edited by J. Wolfrum, H-R. Volpp, R. Rannacher, and J. Warnatz (Springer-Verlag, Heidelberg, 1996), p. 125.
[4] H. Szichman and M. Baer, J. Chem. Phys. **105**, 10380 (1996).
[5] H. Szichman, M. Baer, H-R. Volpp, and J. Wolfrum, J. Phys. Chem. A **102**, 10455 (1998).
[6] J. M. Bowman, J. Phys. Chem. **95**, 4960 (1991).
[7] D. Wang and J. M. Bowman, J. Chem. Phys. **101**, 8646 (1994).
[8] H. Szichman and M. Baer, J. Chem. Phys. **101**, 2081 (1994).
[9] H. Szichman, I. Last, and M. Baer, J. Phys. Chem. **98**, 828 (1994).
[10] M. Baer, I. Last, and H.-J. Loesch, J. Chem. Phys. **101**, 9648 (1994).
[11] M. Gilibert, X. Giménez, F. Huarte-Larrañaga, M. González, A. Aguilar, I. Last, and M. Baer, J. Chem. Phys. **110**, 6278 (1999).
[12] D. Neuhauser and M. Baer, J. Chem. Phys. **90**, 4351 (1989).
[13] H. Szichman, M. Baer, and H. Nakamura, J. Chem. Phys. **107**, 3521 (1997).
[14] R. T. Pack, J. Chem. Phys. **60**, 633 (1974).
[15] J. Tennyson and B. T. Sutcliffe, J. Chem. Phys. **77**, 4061 (1982).
[16] M. E. Rose, *Elementary Theory of Angular Momentum* (Wiley, New York, 1957), Chap. 4.
[17] Z. Bačić and J. C. Light, Annu. Rev. Phys. Chem. **40**, 469 (1989).
[18] J. Z. H. Zhang, S. I. Chu, and W. H. Miller, J. Chem. Phys. **88**, 6233 (1988).
[19] M. Baer and H. Nakamura, J. Chem. Phys. **96**, 6565 (1992).
[20] I. Last, A. Baram, H. Szichman, and M. Baer, J. Phys. Chem. **97**, 7040 (1993).
[21] Z. Bačić and J. C. Light, J. Chem. Phys. **85**, 4594 (1986).
[22] J. Z. H. Zhang and W. H. Miller, J. Phys. Chem. **94**, 7785 (1990).
[23] W. H. Press, S. A. Teukolsky, W. T. Vetterling, and B. P. Flannery, *Numerical Recipes* (Cambridge University Press, Cambridge, MA, 1994), Chap. 2, p. 34.
[24] R. D. Levine and R. B. Bernstein, *Molecular Reaction Dynamics and Chemical Reactivity* (Oxford University Press, Oxford, 1987).

[25] L. B. Harding, G. C. Schatz, and R. A. Chiles, J. Phys. Chem. **76**, 5172 (1982).
[26] X. Zhang, Yi-h. Ding, Ze-s. Li, Xu-ri Huang, and C.-c. Sun, J. Phys. Chem. A **104**, 8375 (2000).
[27] D. L. Baulch, C. J. Cobos, R. A. Cox, C. Esser, P. Frank, T. Just, J. A. Kerr, M. J. Pilling, J. Troe, R. W. Walker, and J. Warnatz, J. Phys. Chem. Ref. Data **21**, 411 (1992).
[28] W. Lange and H. Gg. Wagner, Ber. Bunsenges Phys. Chem. **79**, 165 (1975).
[29] A. H. Laufer and A. M. Bass, J. Phys. Chem. **83**, 310 (1979).
[30] A. M. Relund, F. Shokoohi, H. Reisler, and C. Wittig, Chem. Phys. Lett. **84**, 293 (1981).
[31] H. Okabe, J. Chem. Phys. **75**, 2772 (1981).
[32] T. Koike and K. Morinaga, Bull. Chem. Soc. Jpn. **54**, 529 (1981).
[33] J. H. Kiefer, S. A. Kapsalis, M. Z. Al-Alami, and K. A. Budach, Combust. Flame **51**, 79 (1983).
[34] J. W. Stephens, J. L. Hall, H. Solka, W.-B. Yan, R. F. Curl, and G. P. Glass, J. Phys. Chem. **91**, 5740 (1987).
[35] X. Koshi, N. Nishida, and H. Matsui, J. Phys. Chem. **96**, 5875 (1992).
[36] S. K. Farhat, C. L. Morter, and G. P. Glass, J. Phys. Chem. **97**, 12789 (1993).
[37] B. J. Opansky and S. R. Leone, J. Phys. Chem. **100**, 19904 (1996).
[38] J. Peeters, H. V. Look, and B. Ceuters, J. Phys. Chem. **100**, 15124 (1996).
[39] H.-G. Yu and G. Nyman, J. Chem. Phys. **111**, 3508 (1999).
[40] M. L. Wang, Y. Li, J. Z. H. Zhang, and D. H. Zhang, J. Chem. Phys. **113**, 1802 (2000).
[41] F. Huarte-Larrañaga and U. Manthe, J. Chem. Phys. **113**, 5115 (2000).